

Measurement of the ionization yield of nuclear recoils in liquid argon at 80 and 233 keV

A. BONDAR^{1,2}, A. BUZULUTSKOV^{1,2} ^(a), A. DOLGOV², E. GRISHNYAEV¹, S. POLOSATKIN^{1,2}, L. SHEKHTMAN^{1,2}, E. SHEMYAKINA^{1,2} and A. SOKOLOV^{1,2}

¹ *Budker Institute of Nuclear Physics SB RAS, Novosibirsk, 630090, Russia*
² *Novosibirsk State University, Novosibirsk, 630090, Russia*

PACS 29.40.-n – Radiation detectors

PACS 95.55.Vj – Neutrino, muon, pion, and other elementary particle detectors; cosmic ray detectors

PACS 95.35.+d – Dark matter

Abstract –The energy calibration of nuclear recoil detectors is of primary importance to rare-event experiments such as those of direct dark matter search and coherent neutrino-nucleus scattering. In particular, such a calibration is performed by measuring the ionization yield of nuclear recoils in liquid Ar and Xe detection media, using neutron elastic scattering off nuclei. In the present work, the ionization yield for nuclear recoils in liquid Ar has for the first time been measured in the higher energy range, at 80 and 233 keV, using a two-phase Cryogenic Avalanche Detector (CRAD) and DD neutron generator. The ionization yield in liquid Ar at an electric field of 2.3 kV/cm amounted to 7.8 ± 1.1 and 9.7 ± 1.3 e⁻/keV at 80 and 233 keV respectively. The Jaffe model for nuclear recoil-induced ionization, in contrast to that Thomas-Imel, can probably consistently describe the energy dependence of the ionization yield.

Introduction. – The energy calibration of nuclear recoil detectors is of primary importance to rare-event experiments [1] such as those of direct dark matter search [2–12] and coherent neutrino-nucleus scattering [13, 14]. Such a calibration, in particular in liquid Ar and Xe detection media, is usually performed by measuring the ionization yield and scintillation efficiency of nuclear recoils, using neutron elastic scattering off nuclei (the latter imitating the interaction with dark matter particle or coherently scattered neutrino). While for liquid Xe there is an ample of experimental data on such yields [15–17], little is known about the ionization yield [18, 19] and scintillation efficiency [20] in liquid Ar.

Recently the first results on the ionization yield of nuclear recoils in liquid Ar have been presented, in the lower energy range: at 6.7 keV [18] and 17–57 keV [19]. In the present work, the ionization yield of nuclear recoils in liquid Ar has for the first time been measured at higher energies, at 80 and 233 keV. These results complement those measurements conducted at lower energies and thus might be relevant to the future dark matter search exper-

iments [7, 8] and to thorough understanding of the ionization yield in liquid Ar. The measurements were performed using a dedicated two-phase Cryogenic Avalanche Detector (CRAD) [21] and DD neutron generator. This study was conducted in the course of the development of two-phase CRADs of ultimate sensitivity for rare-event experiments [21], based on thick Gas Electron Multiplier (THGEM) technique [22], with charge [23] and combined charge/optical [24–26] readout.

The ionization yield measured in experiment is defined as follows:

$$Q_y = n_e/E_0 \quad (1)$$

Here n_e is the number of electrons escaping recombination with positive ions; it depends on the energy deposited by a recoil nuclear in the liquid (E_0) and on the electric field in the liquid (\mathcal{E}). n_e is always smaller than the initial number of ion pairs produced in the liquid by a nuclear recoil (N_i). In the absence of a complete recombination model, it is generally accepted that the following parametrization works well [1, 27]:

^(a)Corresponding author. Email: A.F.Buzulutskov@inp.nsk.su

$$n_e = \frac{N_i}{1 + k/\mathcal{E}} \quad (2)$$

where k is a fitting constant.

Equations 1 and 2 are valid for both electron recoils, induced by electron or gamma-ray irradiation, and nuclear recoils; it is conventional to refer to the corresponding recoil energy in units of keVee (electron-equivalent) and keVnr. The goal of the present study is to measure Q_y for nuclear recoils in liquid Ar at certain energies and electric field and to compare it with that calculated using existing theoretical models.

Experimental setup. — The experimental setup was similar to that used in our previous studies of two-phase CRADs in Ar with THGEM-based charge readout [23,28]. In the two-phase CRAD with charge readout, the primary ionization (electron) charge produced in the liquid by a particle, drifts towards a liquid-gas interface under an electric field, where it is emitted into the gas phase and further multiplied with a double-THGEM multiplier, in a proportional (electron-avalanching) mode. The experimental setup included a vacuum-insulated cryostat with a 9 l volume cryogenic chamber. The chamber consisted of a cathode mesh, immersed in a 0.8 cm thick liquid Ar layer, and a double-THGEM assembly with an active area of $10 \times 10 \text{ cm}^2$, placed in the gas phase above the liquid. The detector was operated in a two-phase mode in the equilibrium state, at a saturated vapour pressure of 1.0 atm and at a temperature of 87 K. In this study, the charge gain of the double-THGEM multiplier was equal to 250; the electric field within the liquid was equal to $\mathcal{E} = 2.3 \text{ kV/cm}$. The Ar was purified by an Oxisorb filter, providing an electron life-time of $\geq 13 \mu\text{s}$ in the liquid, corresponding to the electron drift path before attachment of $\geq 5 \text{ cm}$.

The primary ionization charge in liquid Ar was produced by either X-rays from a ^{241}Am source having among others a 59.5 keV line, or DD neutron generator. The detector was irradiated from outside, practically uniformly across the active area, through two Al windows located at the chambers bottom.

To produce neutrons a specially designed neutron generator was used that continuously emitted monoenergetic neutrons (not collimated) with the kinetic energy of 2.45 MeV obtained in the DD fusion reaction [29,30]. The neutron flux was of the order of 10^4 s^{-1} over full solid angle. The neutron generator (operated at 80 kV and wrapped in a 1 cm thick Pb screen to suppress bremsstrahlung gamma-rays) was placed underneath the two-phase CRAD at a distance of about 10 cm from the active volume.

The charge signals from the two-phase CRAD were recorded from the last electrode of the second THGEM using charge-sensitive amplifiers, with an overall time constant of $10 \mu\text{s}$. The signals were digitized and memorized for further off-line analysis with a LeCroy HRO 66Z digital oscilloscope.

The trigger was provided by the signals from the two-phase CRAD itself at a detection threshold equivalent to the energy of 8 keVee, well above the electronic noises. At this threshold the typical detector rate under neutron irradiation was of the order of 10 s^{-1} , well below the DAQ saturation rate limit. Each experimental session was composed of several measurement runs: that with neutron generator on, that with neutron generator off (to measure the cosmic and detector internal backgrounds) and those of the charge-scale and energy-resolution calibration using a 59.9 X-ray line from ^{241}Am source.

In addition, a neutron scintillation counter made of stilbene ($\text{C}_{14}\text{H}_{12}$) was enabled [28]; it was placed close to the CRAD active volume, just underneath the neutron generator. The counter could effectively separate neutrons from gammas using a pulse-shape analysis and thus estimate the gamma-ray background due to (n, γ) reactions in the two-phase CRAD.

Experimental results. — Fig. 1 shows the raw amplitude spectra in the measurement runs of the most successful session: two pulse-height distributions, obtained in the runs when the neutron generator was on and off, are presented. To obtain the real neutron scattering-induced spectrum, the latter should be subtracted from the former. To calibrate the amplitude scale in terms of the primary ionization charge, the detector was also irradiated with X-rays from ^{241}Am source in the calibration runs: see the inset in the figure. In addition in these calibration runs the amplitude resolution of the detector was measured using the 59.5 keV line: it amounted to $\sigma/E=30\%$. The resolution is expected to be reasonably spatially uniform and practically independent of the energy, being mostly defined by the gain non-uniformity over the THGEM area and the fluctuations of the slow component of an electron emission though the liquid-gas interface [31].

In Eq. 1 one should first determine n_e from the spectra of Fig. 1. For this the pulse-height amplitude in the figure should be normalized to that of 59.5 keV peak and then converted to the primary ionization charge. For the latter one should know, in turn, the ionization yield for 59.5 keV X-rays in liquid Ar. Since the experimental data on this quantity were not available in the literature, we conducted a special intermediate study on the ionization yields for electron-equivalent recoils, namely for X-rays and electrons absorbed in liquid Ar and Xe.

The results are presented in Fig. 2, showing the relative (n_e/N_i) and absolute ($Q_y = n_e/E_0$) ionization yields in liquid Ar and Xe as a function of energy. In liquid Xe, where there are enough experimental data in the energy range of interest, the relative ionization yield dependence on energy is perfectly described by a function $n_e/N_i = 1/(1 + a/E_0)$ with a single parameter a . Accordingly, in liquid Ar we used the similar function, firstly, to describe the experimental data and, secondly, to extrapolate the data to the energy point of interest. In liquid Ar however there was a lack of data in the low energy domain. In this

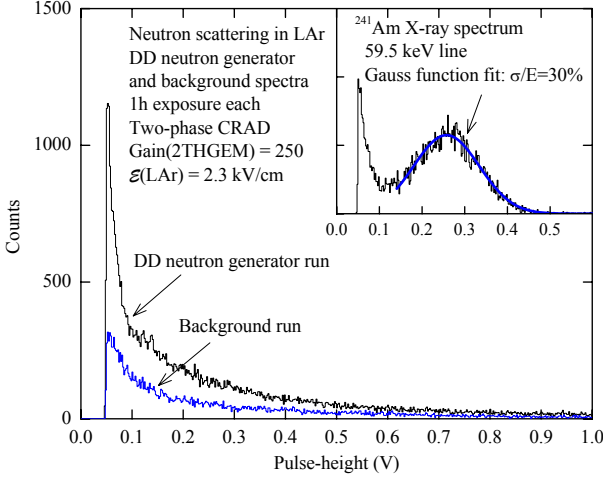


Fig. 1: Pulse-height distributions of the two-phase CRAD signals in the measurement runs when the neutron generator was on (DD neutron generator run) and off (Background run). The run time exposure was 1 h. In the inset, the pulse-height distribution induced by X-rays from ^{241}Am source, in one of the calibration runs, is shown.

domain the data point at 35 keV was obtained ourselves in a dedicated experiment using a small liquid Ar TPC and pulsed X-ray tube, previously used in the study of NIR scintillations in liquid Ar (see [24] and Fig. 7 in ref. [25]); here the X-ray energy was accurately calculated using a dedicated computer program for the given X-ray tube and TPC geometry.

Finally, to calculate n_e (as well as Q_y) from n_e/N_i , we used a W -value (energy needed to produce one ion pair) and its definition, $W = E_0/N_i$: $W = 23.6$ eV in liquid Ar (see table 2 in ref. [1]). The results of this intermediate study are presented in Fig. 2: in particular, for 59.5 keV X-rays the number of detected electrons in liquid Ar at a field of 2.3 kV is predicted to be $n_e = 1640 \pm 50e^-$.

After subtracting the background-run contribution, the amplitude distribution still contains the gamma-ray background, resulted from (n, γ) reactions in surrounding materials. This contribution was experimentally determined using the data from the neutron counter: see Fig. 3. Firstly, the neutron signals were effectively separated from those of gamma-rays applying the pulse-shape analysis (see top-right panel). Then the gamma-ray contribution was determined comparing the neutron and gamma-ray count rates during the experimental session, namely when the neutron generator was on and off (see the bottom panel): it was equal to 15% of the neutron count rate. Finally, the energy spectra for neutrons and gamma-rays were measured in the counter (see the top-left panel). The gamma-ray spectrum here is defined by electron recoils in stilbene from the carbon atoms due to Compton scattering of gamma-rays produced by surrounding H, C, Ar, Fe, Pb, etc nuclei with the energies above 0.6 MeV.

At these photon energies the spectrum of electron recoils

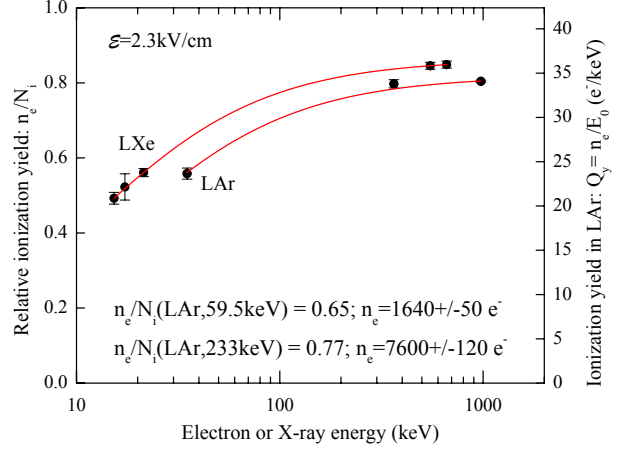


Fig. 2: Relative (left scale) and absolute (right scale) ionization yields in liquid Ar and Xe for electron-equivalent recoils, namely for X-rays and electrons, as a function of the X-ray or electron energy, at an electric field of 2.3 kV/cm. The experimental data points in liquid Xe were obtained from refs. [32] (15.3, 17.3, and 21.4 keV), [33] (550 keV) and [34] (662 keV); in liquid Ar - from the present work (35 keV), from refs. [35] (364 keV) and [33] (976 keV). The data on the constant k of Eq. 2 were used from table 2.6 of ref. [27], if necessary, to calculate the relative ionization yield at a field of 2.3 kV/cm for those experimental data points.

due to Compton scattering at the given recoil energies can be approximated by a linear decreasing function with energy (see Fig. 10.1 in ref. [37]). Accordingly in liquid Ar the gamma-ray contribution due to Compton scattering appeared in the energy spectrum as a long tail extending to higher energies, fitted by a linear decreasing function: see the inset in Fig. 4. The contribution of gamma-ray background determined that way amounted to about 45% of that of neutrons. This is close to that expected from the neutron counter data: the Compton effect in Ar is enhanced in proportion to the atomic number when compared to that in C, i.e. roughly by a factor of 3, while the neutron-nucleus cross-sections almost do not change.

Fig. 4 shows the desired ionization charge spectrum in liquid Ar induced by nuclear recoils due to neutron scattering; the spectrum is obtained from Fig. 1 using 59.5 keV X-ray line calibration and subtracting the background-run and gamma-ray contributions. The next step is to compare this experimental spectrum to that of theoretical.

The theoretical spectrum was computed using simulation code *Scattronix* developed in the Budker INP [38] and differential cross-sections of elastic and inelastic neutron scattering [39]. For the ^{40}Ar nuclei irradiated by neutrons with the energy of 2.45 MeV it is shown in Fig. 5. One can see that the maximum recoil energy for the Ar nuclei, achieved for backward neutron scattering at 180° , is 233 keV. The convolution of the theoretical spectrum with the energy resolution of the two-phase CRAD obtained in experiment (30%), is also shown; just this spectrum should be compared to that of experimental. Two components of

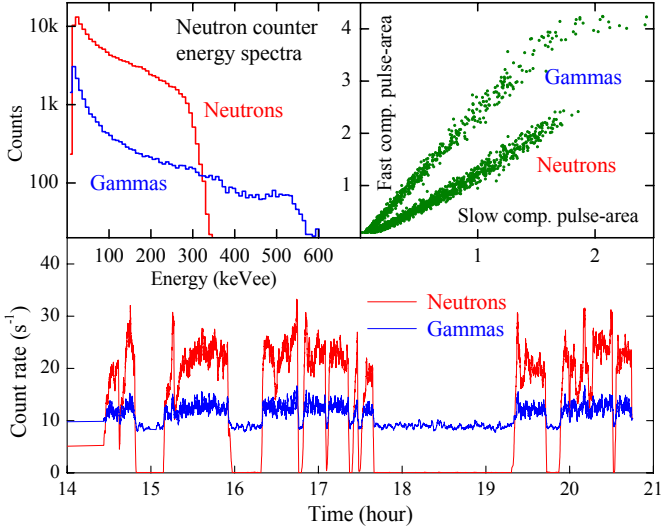


Fig. 3: Data from the neutron counter. Top-right panel: neutron/gamma-ray separation using the fast and slow pulse components of the stilbene-scintillator signal. Bottom panel: the neutron and gamma-ray count rate evolution during the experimental session with several measurement runs when the neutron generator was either on or off. Top-left panel: the energy distributions of the neutron- and gamma-ray-induced events, the contribution of the latter being equal to 15% of that of the former. Here the energy scale calibration was performed using the neutron spectrum end-point, corresponding to proton recoils with the energy of 2.45 MeV, and the scintillation quench factor in stilbene for protons of 0.13 [36].

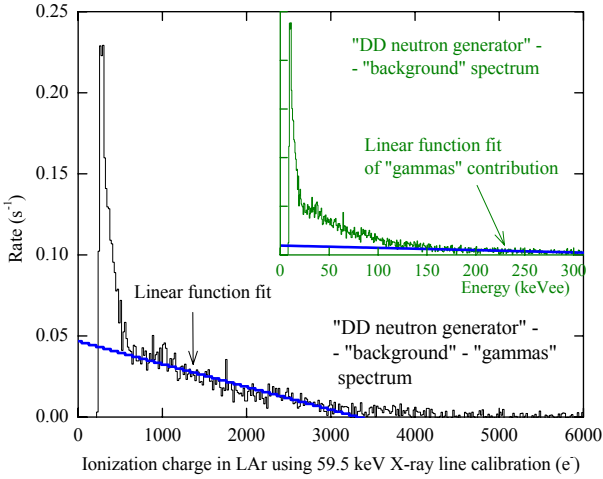


Fig. 4: Ionization charge distribution in liquid Ar induced by nuclear recoils due to neutron scattering, at an electric field of 2.3 kV/cm, obtained from Fig. 1 using 59.5 keV X-ray line calibration and subtracting background-run and gamma-ray contributions. In the inset, the energy distribution is shown after subtracting the background-run contribution, but before subtracting the gamma-ray contribution, the latter being fitted by a linear decreasing function. Here the energy scale calibration was performed using the 59.5 keV X-ray line.

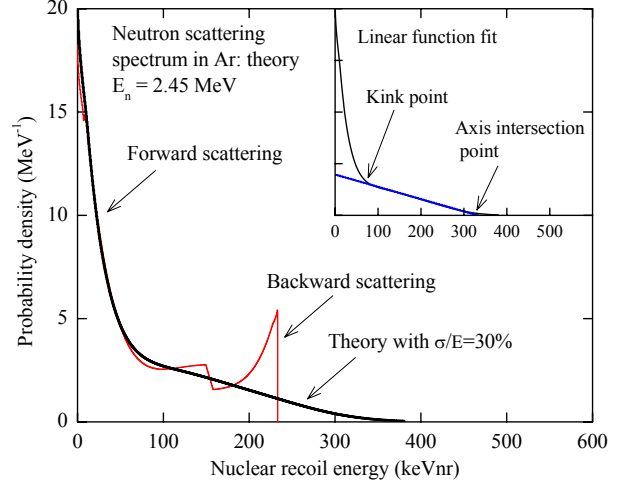


Fig. 5: Nuclear recoil energy distribution induced by scattering of neutrons with the energy of 2.45 MeV off ^{40}Ar nuclei, computed theoretically (red line). The convolution of the theoretical spectrum with the energy resolution of the two-phase CRAD obtained in experiment (30%), is also shown (black line). In the inset, two characteristic points of the spectrum with respect to the linear function fit of the backward scattering component are indicated: that of the axis intersection at the spectrum end-point and that of the spectrum kink at the transition between the forward and backward scattering components.

neutron scattering are distinctly seen in the figure: those of the forward and backward scattering, respectively represented in the distribution by the peak at lower energies and the shoulder at higher energies. These two components are well reproduced in the experimental spectrum in Fig. 4. It is interesting that the backward scattering component (the shoulder) in both the experimental and theoretical spectra is well approximated by a linear function: see Fig. 4 and the inset in Fig. 5.

One cannot directly fit the theoretical spectrum to that of experimental in order to obtain the ionization yield, due to the unknown energy dependence of the yield. On the other hand, one can select the characteristic points at certain nuclear recoil energies in both the experimental and theoretical spectra and calculate the ionization yield at these points according to Eq. 1. Namely at these points, one should divide the ionization charge value (in the experimental spectrum) by that of the nuclear recoil energy (in the theoretical spectrum). Fortunately, the mathematically justified choice of two such points can be done with respect to the linear function fit of the backward scattering component (see the inset in Fig. 5). The first point, characterizing the spectrum end-point, is that of the horizontal axis intersection of the linear function. The second point, characterizing the transition between the forward and backward scattering components, is that of the spectrum kink, defined as the spectrum deflection from the linear function fit of the backward component. The nuclear recoil energies which should be attributed to these

Table 1: Ionization yields (Q_y) of nuclear recoils in liquid Ar with uncertainties measured at an electric field of 2.3 kV/cm

Energy (keV)	Q_y (e^-/keV)	Statistical	Systematic	Total error
233	9.7	0.29	1.3	1.3
80 ± 2	7.8	0.24	1.05	1.1

two points are those of 233 keV and 80 ± 2 keV, respectively.

Consequently, the ionization yield values at these two energies measured in that way are as follows: $Q_y = 9.7 \pm 1.3 e^-/\text{keV}$ at 233 keV and $Q_y = 7.8 \pm 1.1 e^-/\text{keV}$ at 80 keV. These are presented in Table 1, showing also the appropriate statistic and systematic uncertainties and their quadratic sum (total error).

In addition to the ionization yield, the ionization efficiency, sometimes called the ionization quench factor, can be determined. The ionization efficiency is defined by analogy with the scintillation efficiency, i.e. as the ratio of the ionization yield of nuclear recoils ($Q_{y,nr}$) to that of electron-equivalent recoils ($Q_{y,ee}$), at the same energy: $L_{ion} = Q_{y,nr}/Q_{y,ee}$. Combining the data of Table 1 and Fig. 2, one can obtain that L_{ion} amounts to 0.30 ± 0.04 at 233 keV and 0.27 ± 0.04 at 80 keV.

Accordingly, one may conclude that the ionization yields of nuclear recoils in liquid Ar at energies above 80 keV might be relatively large, reaching values of the order of $10 e^-/\text{keV}$ at electric fields exceeding 2 kV/cm. In addition, the ionization quench factor in these conditions is about 30%.

Comparison with other experiments and with theoretical models. – In Fig. 6 our data on the ionization yield are compared to those of ref. [18] measured at 6.7 keV. The data point of the latter was obtained at a close field value, at 2.13 kV/cm; it was extrapolated to that of 2.3 kV/cm, using the measured field dependence of ref. [18]. One can see that the experimental data look compatible in terms of the absolute value of the ionization yield. In addition, the ionization yield looks to be an increasing function with energy.

On the other hand, the ionization yield measured at lower energies, below 57 keV, in another work in the field [19], was reported to be a decreasing function with energy, in contrast to our results. The explanation of such a discrepancy might be a non-monotonic energy dependence of the ionization yield, predicted in some computer simulation models [40].

Basically there are two theoretical models that can describe the recombination effect in liquid noble gases and consequently the energy and field dependence of the ionization yield of nuclear recoils: that of Thomas-Imel [41, 42] and that of Jaffe [43, 44].

One can see in Fig. 6 that the energy dependence

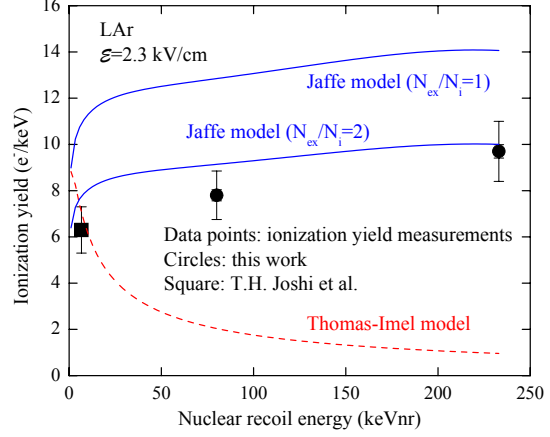


Fig. 6: Ionization yield of nuclear recoils in liquid Ar at 2.3 kV/cm as a function of the energy, measured in the present work (circles) and in T.H. Joshi et al. [18] (square). The theoretical predictions for the ionization yield are also shown, obtained in the frame of Thomas-Imel (dashed curve) and Yaffe (solid curve) models.

measured in experiment fully contradicts to Thomas-Imel model [41, 42] that predicts the decreasing function with energy for the ionization yield. In this model,

$$n_e = \frac{N_i}{\xi} \ln(1 + \xi); \quad \xi = \frac{N_i C}{\mathcal{E}^b}; \quad N_i = \frac{f E_0}{W_s^{min}} (1 + N_{ex}/N_i) \quad (3)$$

$$Q_y = \frac{f}{W_s^{min}} (1 + N_{ex}/N_i) \frac{\ln(1 + \xi)}{\xi} \quad (4)$$

Here b and C are fitting constants, their values being taken from ref. [18] for the data point at 6.7 keV; $W_s^{min} = 19.5$ eV is the minimum energy required to produce a scintillation photon (i.e. to produce excitation or ionization) in liquid Ar [1]. The ratio of the number of excitations to that of ionizations was taken the same as in [18]: $N_{ex}/N_i = 0.2$.

f is the Lindhard factor (also called quench factor), characterizing the nuclear recoil collisions; it is defined as the energy fraction transferred to ionization (E_i) and excitation (E_{ex}):

$$f = (E_i + E_{ex})/E_0 \quad (5)$$

For electron recoils it is equal to unity. For nuclear recoils it can be calculated in two ways: either taking the calculations of Linhard et al. [45] or using a SRIM computer program [46] developed for low energy ion collisions. In the present work we used the second method.

In contrast to Thomas-Imel model, the Jaffe model [43] in its compact form [44] predicts the increasing function with energy for the ionization yield: see Fig. 6. In this form the model has a Birks-like equation [44],

$$n_e = \frac{N_i}{1 + k_B (dE/dx)/\mathcal{E}} \quad (6)$$

Here k_B is a constant; it was determined from the field dependence of the data of ref. [18] at 6.7 keV. The stopping power (energy losses) for excitation and ionization, dE/dx , was calculated using the SRIM program [46].

The equation for the ionization yield in the frame of this Jaffe model was derived ourselves from Eq. 6,

$$Q_y = \frac{f}{[1 + k_B(dE/dx)/\mathcal{E}][E_g + E_{ph}(N_{ex}/N_i)]} \quad (7)$$

using Eq. 5, where $E_i = N_i E_g$ and $E_{ex} = N_{ex} E_{ph}$ (see section 4 in ref. [1] for more details of the energy balance in liquid noble gases). Here $E_g \simeq 14.2$ eV is the band gap in liquid Ar, which we adopt equal to that of solid Ar (see table 2 in ref. [1]); $E_{ph}=9.7$ eV is the average energy of scintillation photon. In the lack of theoretical and experimental data for liquid Ar, the ratio N_{ex}/N_i can be taken here either equal to that measured for nuclear recoils in liquid Xe [47], namely $N_{ex}/N_i=1$, or 10 times greater than the ratio for electron recoils in liquid Ar (in the same way as it was for Xe - see table 2 in [1]), namely $N_{ex}/N_i=2$. One can see that the Jaffe model can probably consistently describe the experimental data in terms of the energy dependence, and even in terms of the absolute values in the latter case.

Conclusions. – In the present work, the ionization yield of nuclear recoils in liquid Ar has for the first time been measured at higher energies, namely at 80 and 233 keV, using a two-phase Cryogenic Avalanche Detector (CRAD) and DD neutron generator. The ionization yield in liquid Ar at an electric field of 2.3 kV/cm amounted to 7.8 ± 1.1 and 9.7 ± 1.3 e⁻/keV at 80 and 233 keV respectively; the ionization quench factor amounted to 0.27 ± 0.04 and 0.30 ± 0.04 respectively. The Jaffe model can probably consistently describe the energy dependence of the ionization yield, in the energy range of 6-230 keV, in contrast to that of Thomas-Imel. The results of such a study is relevant to the energy calibration of liquid noble gas detectors for dark matter search experiments and understanding of the ionization yield in liquid Ar.

* * *

This work was supported in part by the Ministry of Education and Science of Russian Federation and by the grants of the Government of Russian Federation (11.G34.31.0047) and the Russian Foundation for Basic Research (12-02-91509-CERN-a).

REFERENCES

- [1] CHEPEL V. and ARAUJO H., *JINST*, **8** (2013) R04001.
- [2] ANGLE J. ET AL., *Phys. Rev. Lett.*, **107** (2011) 051301.
- [3] APRILE E. ET AL., *Phys. Rev. Lett.*, **109** (2012) 181301.
- [4] AKIMOV D. ET AL., *Phys. Lett. B*, **709** (2012) 14.
- [5] BENETTI P. ET AL., *Astropart. Phys.*, **28** (2007) 495.
- [6] AKERIB D.S. ET AL., *Phys. Rev. Lett.*, **112** (2014) 091303.
- [7] BADERTSCHER A. ET AL., *JINST*, **8** (2013) C09005.
- [8] ALEXANDER ET AL., *JINST*, **8** (2013) C11021.
- [9] BERNABEI R. ET AL., *Eur. Phys. J. C*, **67** (2010) 39.
- [10] AALSETH C.E. ET AL., *Phys. Rev. D*, **88** (2013) 012002.
- [11] ANGLOHER G. ET AL., *Eur. Phys. J. C*, **72** (2012) 1971.
- [12] ANGLE J. ET AL., *Phys. Rev. Lett.*, **111** (2013) 251301.
- [13] HAGMANN C. and BERNSTEIN A., *IEEE Trans. Nucl. Sci.*, **51** (2004) 2151.
- [14] AKIMOV D. ET AL., *JINST*, **4** (2009) P06010.
- [15] MANZUR A. ET AL., *Phys. Rev. C*, **81** (2010) 025808.
- [16] HORN M. ET AL., *Phys. Lett. B*, **705** (2011) 471.
- [17] PLANTE G. ET AL., *Phys. Rev. C*, **84** (2011) 045805.
- [18] JOSHI T.H. ET AL., *Phys. Rev. Lett.*, **112** (2014) 171303.
- [19] CAO H. ET AL., Eprint arXiv:1406.4825, 2014.
- [20] GASTLER D. ET AL., *Phys. Rev. C*, **85** (2012) 065811.
- [21] BUZULUTSKOV A., *JINST*, **7** (2012) C02025.
- [22] BRESKIN A. ET AL., *Nucl. Instr. Meth. A*, **598** (2009) 107.
- [23] BONDAR A. ET AL., *JINST*, **8** (2013) P02008.
- [24] BUZULUTSKOV A., BONDAR A. and GREBENUK A., *EPL*, **94** (2011) 52001.
- [25] BONDAR A. ET AL., *JINST*, **7** (2012) P06014.
- [26] BONDAR A. ET AL., *Nucl. Instr. Meth. A*, **732** (2013) 213.
- [27] BARABASH A.S. and BOLOZDYNYA A.I., *Liquid ionization detectors* (Energoatomizdat, Moscow) 1993 (In Russian).
- [28] BONDAR A. ET AL., *JINST*, **9** (2014) C08020.
- [29] BONDAR A.E. ET AL., *Bulletin NSU: Physics*, **8**, issue 3 (2013) 27 (in Russian).
- [30] GRISHNYAEV E.S. and POLOSATKIN S.V., *Atomic Energy*, **113**, No. 5 (2013) 345 (in Russian).
- [31] BONDAR A. ET AL., *JINST*, **4** (2009) P09013.
- [32] VORONOVA T.YA. ET AL., *Journal of Technical Physics*, **59**, issue 7 (1989) 186 (in Russian).
- [33] SHIBAMURA E. ET AL., *Nucl. Instr. Meth.*, **131** (1975) 249.
- [34] OBODOVSKIY I.M. and POKACHALOV S.G., *Physics of Low Temperatures*, **5**, No. 8 (1979) 829 (in Russian).
- [35] SCALLETAR R.T. ET AL., *Phys. Rev.*, **25** (1982) 2419.
- [36] SHIMIZU Y. ET AL., *Nucl. Instr. Meth. A*, **496** (2003) 347.
- [37] KNOLL G.F., *Radiation Detection and Measurement* (Wiley) 2010.
- [38] GRISHNYAEV E.S., DOLGOV A.D. and POLOSATKIN S.V., *Bulletin NSU: Physics*, **8**, issue 3 (2013) 39 (in Russian).
- [39] CHADWICK M. ET AL., *Nuclear Data Sheets*, **107** (2006) 2931.
- [40] SZYDAGIS M. ET AL., *JINST*, **8** (2013) C10003.
- [41] THOMAS J. and IMEL D.A., *Phys. Rev. A*, **36** (1987) 614.
- [42] SZYDAGIS M. ET AL., *JINST*, **6** (2011) P10002.
- [43] JAFFE G., *Ann. Phys.*, **42** (1913) 303.
- [44] ACCIARRI R. ET AL., *JINST*, **8** (2013) P08005, and references therein.
- [45] LINDHARD J. ET AL., *Integral equations governing radiation effects* (I kommission hos Munksgaard, Copenhagen) 1963.
- [46] ZIEGLER F., BIRSACK J.P. and LITTMARK U., *The Stopping and Range of Ions in Solids* (Pergamon Press, New York) 1985. <http://srim.org/>
- [47] SORENSEN P. and DAHL C.E., *Phys. Rev. D*, **83** (2011) 063501.